

Synthesis, Characterization, and Catalytic Properties of Hollow γ-Fe_2O_3 Spheres toward Liquid-Phase Oxidation Using Hydrogen Peroxide

Kohsuke Mori, Isamu Tanimura, and Hiromi Yamashita*

Division of Materials and Manufacturing Science, Graduate School of Engineering, Osaka University, 2-1 Yamada-oka, Suita, Osaka 565-0871

Received May 6, 2010; E-mail: yamashita@mat.eng.osaka-u.ac.jp

Hollow γ-Fe_2O_3 nanospheres were synthesized using carboxylated polystyrene spheres as a core template by thermal treatment followed by calcination. The obtained material was characterized by FT-IR, N_2 adsorption–desorption, TEM, XRD, and Fe K-edge XAFS measurements. The size of the hollow γ-Fe_2O_3 nanospheres were about 400–500 nm, which was assembled from primary particles with a size of approximately 10–20 nm. The phase transition of the composed particles from magnetite (Fe_3O_4) to maghemite (γ-Fe_2O_3) was identified after calcination in the presence of O_2 at relatively low temperature. The hollow γ-Fe_2O_3 acted as an efficient heterogeneous catalyst for the liquid-phase selective oxidation of 1-phenylethanol using hydrogen peroxide (H_2O_2) as an oxidant. It exhibited enhanced catalytic activity compared to its bulk counterpart and also showed higher selectivity than nanosized γ-Fe_2O_3. Recovery of the hollow γ-Fe_2O_3 nanospheres from the reaction mixture could be attained by applying an external permanent magnet, and the spent catalyst could be recycled without any appreciable loss of its inherent catalytic ability.

Nanoscale metal particles and metal oxide particles have attracted a great deal of attention as potentially advanced materials possessing unique electronic, optic, and magnetic properties as well as catalytic functions.[1] Scientists in the field of catalytic chemistry have expected that these metal and metal oxide nanoparticles (NPs) would provide unique catalysis that cannot be achieved with mononuclear metal complexes and heterogeneous bulk phase because of quantum size effects and large surface area-to-volume ratio,[2] however there is often a trade-off between stability and catalytic activity. Unsupported free NPs frequently exhibit exceptionally high initial catalytic activity because of higher surface area, low-coordination site, and surface vacancies, but they are usually unstable and the coagulation of NPs during reaction is unavoidable. In order to overcome the above drawbacks, catalytic NPs have been conventionally synthesized and isolated as individual particles in the presence of protective ligands ranging from small organic molecules to large polymers.[3] Recently, novel systems such as dendrimers,[4] block copolymer nanospheres,[5] and crosslinked lyotropic liquid crystals[6] have been employed to encapsulate NPs. Unfortunately, a slow penetration of reactants into the clump of the above bulky ligands generally results in low catalytic activity despite the stability toward agglomeration.

In the last few decades, hollow spheres with nanometer to micrometer dimensions have aroused intense research interest not only for their unique functions, but also for their wide range of applications in various fields including drug delivery, sensing, and photonic crystals.[7] Hollow spheres composed of nanometer-sized metal particles represent a new class of promising catalyst bridging the gap between metal NPs and bulk counterparts.[8] The high surface area of the hollow spheres originating from the nanoparticulate nature in the shell region, which is much larger than that of dense spheres of the same diameter, is responsible for the high catalytic activity. Self-supporting capacity can offer high durability as well as smooth reaction under ligand-free conditions. Moreover, metal atoms can be highly dispersed within the unique interior void spaces, which also create a nanosized reactor that may enhance the catalytic efficiency and be easily separated from the reaction mixture. The synthesis often relies on templating approaches, in which various sacrificial templates including latex spheres, resin spheres, microemulsions, polymer micelles, and block copolymers are used to create a hollow structure.[9]

In this study, we describe the fabrication of maghemite (γ-Fe_2O_3) hollow spheres with submicrometer dimensions assembled by NPs and catalytic evaluation in liquid-phase reactions. γ-Fe_2O_3 has attracted technological interest because it is readily synthesized and it exhibits interesting chemical and magnetic properties. Up to now, size-controlled syntheses of γ-Fe_2O_3 have been developed.[10] A variety of γ-Fe_2O_3 structures such as nanocubes,[11] rings,[12] and wire[13] have also been fabricated. There has been a dramatic increase in interest because the magnetic properties are strongly dependent on the size and morphology of the particles; however their catalytic applications have not been investigated so far.

Experimental

Materials. $FeCl_2 \cdot 4H_2O$, KNO_3, ethylene glycol, and hexamethylenetetramine (hmta) were purchased from Wako Pure Chemical Ind., Ltd. Carboxylated polystyrene latex sphere was obtained from Alfa Aesar. Bulk Fe_3O_4, γ-Fe_2O_3, and nano-γ-Fe_2O_3 were prepared according to reported methods.[14,15] Solvents and all commercially available organic compounds for catalytic reactions were purified by standard procedures.

Published on the web September 2, 2010; doi:10.1246/bcsj.20100130

The Synthesis of Hollow Iron Oxides. A 2.5% aqueous solution of carboxylated polystyrene (PS) latex microspheres (350 nm) were dispersed in 150 mL water and sonicated to prevent aggregation. $FeCl_2 \cdot 4H_2O$ (3.5 mmol), KNO_3 (1.1 mmol), and hmta (14.3 mmol) were dissolved in an aqueous ethylene glycol (EG) solution (EG/water = 50/150 mL) and the resulting solution was added to the aqueous solution of carboxylated PS spheres and then heated at 353 K under Ar atmosphere. After 3 h, the obtained precipitate was filtered, washed repeatedly with ethanol and deionized water and dried under vacuum overnight to give Fe_3O_4-coated PS spheres as a dark green powder. The sample was then calcined at 723 K for 5 h under Ar atmosphere to remove the core PS from the materials, giving a hollow Fe_3O_4 as a black powder. Finally, the resulting material was further treated with air at 473 K for 2 h, affording a hollow γ-Fe_2O_3 as a reddish-brown powder.

Characterization. Powder X-ray diffraction patterns were recorded using a Rigaku RINT2500 diffractometer with Cu Kα radiation ($\lambda = 1.5406$ Å). BET surface area measurement was performed using a BEL-SORP max (Bel Japan, Inc.) at 77 K. The sample was degassed in vacuum at 423 K prior to data collection. Infrared spectra were obtained with a JASCO FTIR-6100. Samples were diluted with KBr and compressed into thin disk-shaped pellets. TEM micrographs were obtained with a Hitachi Hf-2000 FE-TEM equipped with a Kevex energy-dispersive X-ray detector operated at 200 kV. Fe K-edge XAFS spectra were recorded using fluorescence-yield collection at the beam line 01B1 station with an attached Si(311) monochromator at SPring-8, JASRI, Harima, Japan (prop. No. 2009B1127). In a typical experiment, the sample was loaded into an in situ cell with plastic windows. The EXAFS data were examined by an EXAFS analysis program, Rigaku EXAFS. The pre-edge peaks in the XANES regions were normalized for atomic absorption, based on the average absorption coefficient of the spectral region. Fourier transformation (FT) of k^3-weighted normalized EXAFS data was performed over the 3.5 Å $< k/$Å$^{-1} <$ 11 Å range to obtain the radial structure function.

A Typical Example for the Liquid-Phase Oxidation. Into a reaction vessel with a reflux condenser were placed Fe catalyst (0.01 g), 1-phenylethanol (2.0 mmol), acetonitrile (10.0 mL), and 30% H_2O_2 (1.0 mL). The resulting mixture was stirred at 353 K. The progress of reaction was monitored by GC analysis using an internal standard for 48 h. The magnetically recovered catalyst was washed with 10 mL of ethanol and 10 mL of H_2O before reuse. The recycling procedures were repeated in the same manner as in the first run. Analytical GC was performed with a Shimadzu GC-14B with flame ionization detector equipped with TC-5HT columns.

Results and Discussion

Scheme 1 shows a schematic illustration of the procedure to synthesize hollow Fe_3O_4 (magnetite) and γ-Fe_2O_3 (maghemite) spheres. In a preliminary experiment, we employed unfunctionalized PS spheres as a core template. However, this trial was not successful. The hollow structures were scarcely confirmed by TEM images because of the independent growth of iron oxide phase. Therefore, we utilized carboxylated PS spheres as an alternative. At first, carboxylated PS spheres were

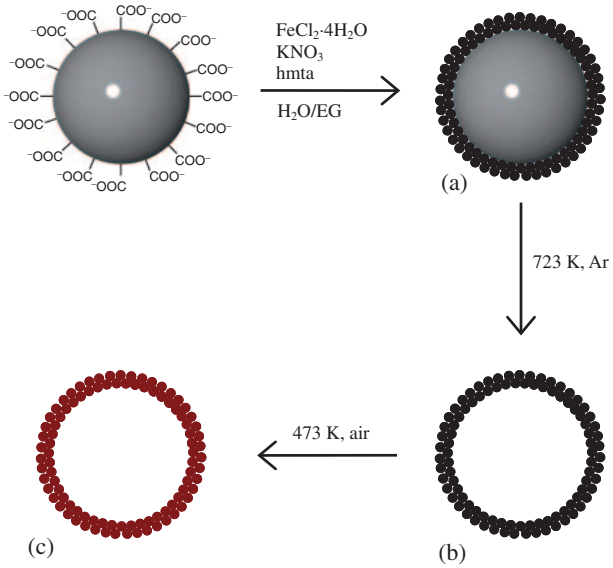

Scheme 1. Synthetic procedure of (a) Fe_3O_4-coated PS sphere, (b) hollow Fe_3O_4, and (c) hollow γ-Fe_2O_3 using carboxylated PS spheres as a template.

introduced into an aqueous EG solution of the ferrous salt, KNO_3, and hmta. The resultant solution was heated to produce Fe_3O_4-coated PS spheres, which were calcined under Ar atmosphere to remove the structurally incorporated template, giving a hollow Fe_3O_4 as a black powder. Finally, the resulting material was calcined under air, affording a hollow γ-Fe_2O_3 as a reddish-brown powder. This color change originates from the transformation of Fe_3O_4 phase into γ-Fe_2O_3. It is well-known that the precipitation of ferrous ions in a basic aqueous solution first gives Fe_3O_4 particles, which can be easily oxidized to γ-Fe_2O_3 at relatively low temperature, and subsequently transformed into α type at high oxidation temperature.[16] The obtained hollow nanospheres are also expected to be a single magnetic domain and exhibit a magnetic moment only in the presence of a magnetic field, indicating a superparamagnetic nature.[17] When the magnetic field is removed, the particles immediately return to their nonmagnetic state.

As shown in Figure 1a, peaks due to the methylene and aromatic ring ν(C–H) stretch vibration in PS were observed at around 3029 and 2925 cm^{-1} in the FT-IR spectrum of the Fe_3O_4-coated PS spheres. Two peaks at around 700–760 cm^{-1} can be ascribed to the stretching vibration of the monoreplacement in the phenyl ring group of PS. The above peaks completely disappeared after the heat treatment, revealing that PS was largely removed (Figure 1b).

N_2 adsorption–desorption of the hollow Fe_3O_4 and γ-Fe_2O_3 showed a type III isotherm with a slight hysteresis loop in the range 0.8–1.0 P/P_0, maybe reflecting the presence of macropores (>50 nm). The Brunauer–Emmett–Teller (BET) surface area (S_{BET}) and pore volume (V_p) of the hollow Fe_3O_4 ($S_{BET} = 41.1$ m^2 g^{-1} and $V_p = 0.44$ cm^3 g^{-1}) and hollow γ-Fe_2O_3 ($S_{BET} = 36.2$ m^2 g^{-1} and $V_p = 0.29$ cm^3 g^{-1}) after calcinations were found to be much larger than those of the as-synthesized Fe_3O_4-coated PS spheres ($S_{BET} = 21.6$ m^2 g^{-1} and $V_p = 0.16$ cm^3 g^{-1}), respectively. This is clear evidence for the formation of hollow structure after the removal of the PS

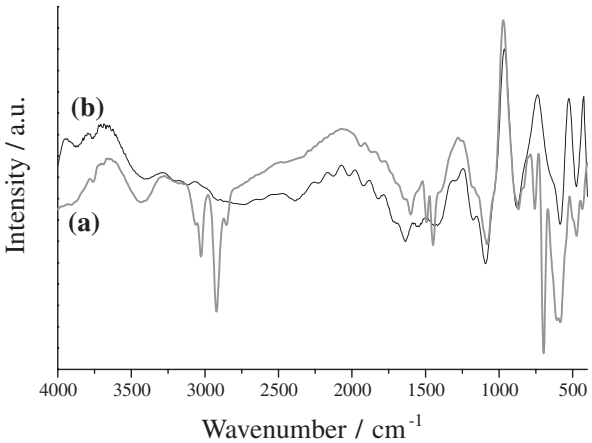

Figure 1. IR spectra for (a) Fe_3O_4-coated PS spheres and (b) hollow γ-Fe_2O_3.

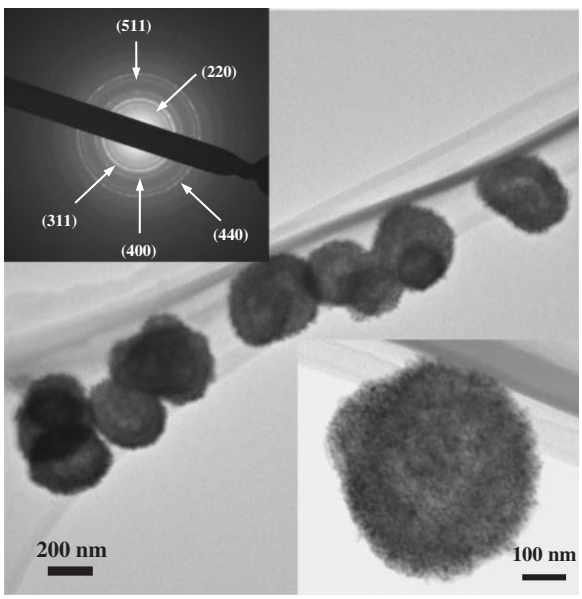

Figure 2. TEM image and electron diffraction pattern of hollow γ-Fe_2O_3.

sphere, and which is stable even after the phase transition from Fe_3O_4 to γ-Fe_2O_3 by oxidation in the presence of O_2.

Figure 2 shows TEM images of the hollow γ-Fe_2O_3 spheres, in which we can observe hollow spheres with a pale center region in contrast to a dark edge. The particle size was determined to be about 400–500 nm, while shell thickness is estimated to be approximately 40–50 nm. Thus, the diameter of inner macropores were about 300–400 nm, which is consistent with that of the employed PS microsphere template. From the single hollow sphere, it can be seen that the hollow sphere is composed of irregular shaped primary particles of approximately 10–20 nm in size. The diffraction patterns exhibited atomic lattice fringes corresponding to the (220), (311), (400), (511), and (440) planes of γ-Fe_2O_3, respectively, which is consistent with the results of XRD analysis as described below.

The XRD patterns of the synthesized samples are shown in Figure 3. Fe_3O_4-coated PS sphere and hollow Fe_3O_4 exhibited clear peaks due to Fe_3O_4 phase at around 30.1, 35.4, 43.1, 53.6,

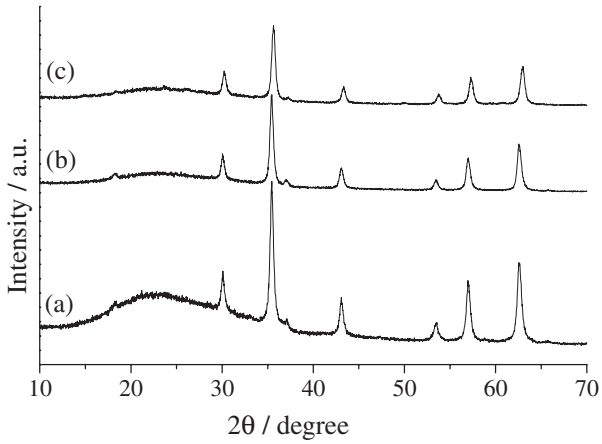

Figure 3. XRD patterns of (a) Fe_3O_4-coated PS spheres, (b) hollow Fe_3O_4, and (c) hollow γ-Fe_2O_3.

57.1, and 62.7°, corresponding to the (220), (311), (400), (422), (511), and (440) reflections, respectively. Distinguishing between Fe_3O_4 and γ-Fe_2O_3 phase by XRD is quite difficult because of the same inverse spinel structure and similarity in their d spacing.[18] As will be mentioned later, the detail characterization of iron oxides can be done by Fe K-edge X-ray absorption fine structure (XAFS). However, the peaks of the hollow γ-Fe_2O_3 slightly shifted to higher angle. All peak positions and relative intensities match well with those of commercial γ-Fe_2O_3, indicating that the oxidation of Fe_3O_4 in the presence of O_2 leads to γ-Fe_2O_3.[19] The average crystalline size of iron oxides were calculated to be 24.4, 23.8, and 21.7 nm in the Fe_3O_4-coated PS sphere, hollow Fe_3O_4 and hollow γ-Fe_2O_3 by applying Scherrer's equation for (311) reflection. These values are well matched with primary particles constituting hollow shell structures. Other iron oxide phases such as α-Fe_2O_3 and metallic bcc-Fe nanoparticles are apparently not involved.

XAFS measurement is also an ideal technique to probe the chemical and structural environment of iron surroundings.[20] Figure 4A shows the Fe K-edge X-ray absorption near-edge structure (XANES) spectra. The edge position (measured at the half-height of the edge jump) depends on the electronic charge of iron ion, and the hollow γ-Fe_2O_3 have higher X-ray absorption edge energy than those of the Fe_3O_4-coated PS spheres and hollow Fe_3O_4 including Fe^{2+} and Fe^{3+}. Thus the hollow γ-Fe_2O_3 appears to be in an electron-deficient state.

In addition to the electronic state, one can get more information about the coordination geometry from the pre-edge region. Fe_3O_4 belongs to the inverse spinel cubic structure family with nonequivalent Fe positions in the unit cell (AB_2O_4).[21] The "A" sites (occupied by Fe^{3+} ion) involve tetrahedral (T_d) coordination, while "B" sites (equally populated by Fe^{3+} and Fe^{2+} ions) have octahedral (O_h) coordination. On the other hand, the structure of γ-Fe_2O_3 is related to the inverse spinel structure of Fe_3O_4 with cation vacancies. The structure can be represented as $(Fe^{3+})[Fe_{5/3}{}^{3+}V_{1/3}]O_4$, in which Fe^{3+} refers to T_d coordination, $Fe_{5/3}$ designates O_h coordination, and $V_{1/3}$ denotes a cation vacancy with O_h coordination.[22] A weak pre-edge peak is mainly due to the quadrupole transition from 1s to 3d orbitals, which is forbidden by dipole

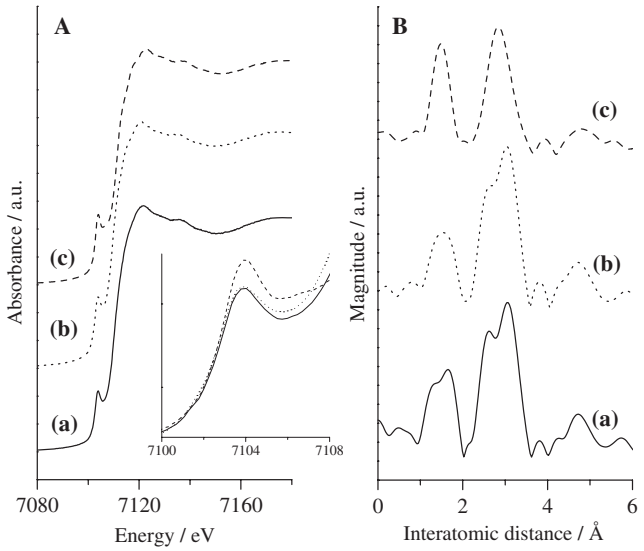

Figure 4. (A) Fe K-edge XANES spectra and (B) FT-EXAFS spectra for (a) Fe_3O_4-coated PS spheres (solid line), (b) hollow Fe_3O_4 (dot line), and (c) hollow γ-Fe_2O_3 (dash line). Inset shows the pre-edge region of the spectra.

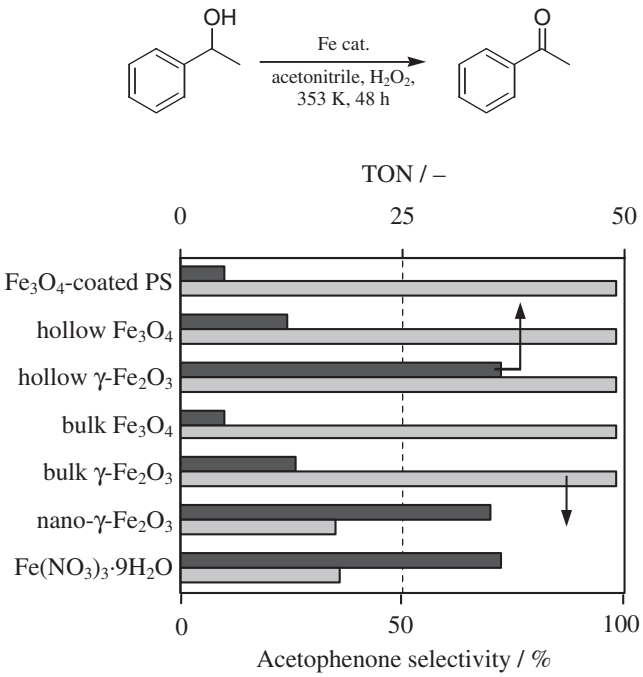

Figure 5. TON and acetophenone selectivity for the oxidation of 1-phenylethanol using H_2O_2.

selection rules in the case of perfect O_h symmetry around an iron atom.[23] The intensity of the pre-edge peak increases with progressive distortion from perfect O_h symmetry and with the contribution of T_d site.[24] As shown in the inset in Figure 4A, the pre-edge peaks of the hollow γ-Fe_2O_3 are relatively strong compared to those of Fe_3O_4 samples, which can be explained by the distortion of the O_h coordinated Fe^{3+} and/or the presence of an additional T_d coordinated Fe^{3+} in the nanosized γ-Fe_2O_3 inverse spinel structure induced by vacant sites.

The Fourier transforms (FT) of Fe K-edge EXAFS data are depicted in Figure 4B. Again, the peak of the hollow γ-Fe_2O_3 differed from those of the Fe_3O_4-coated PS spheres and hollow Fe_3O_4. In particular, the intensity of the second peaks for the hollow γ-Fe_2O_3 is significantly weakened. This peak is attributable to the contiguous Fe–O–Fe bonds due to face-, edge-, vertex-sharing FeO_6 octahedra. The reduced intensity of the hollow γ-Fe_2O_3 in this region can be explained by the structural disorder in primary particles.[25] This peak lowering effect and the differences in electron deficiency of the iron oxides shown by X-ray absorption edge energy can be taken as evidence of formation of Fe_3O_4 and its successful conversion to γ-Fe_2O_3.

Hydrogen peroxide (H_2O_2) is a safe and preferable oxidant from an environmental view point because hydrogen peroxide is converted into water by releasing an oxygen atom to a substrate.[26] Thus, the selective oxidation of organic compounds using H_2O_2 is of great significance in manufacturing many kinds of fine chemicals, agrochemicals and pharmaceutical intermediates. We explored the potential catalytic ability of the hollow iron oxides in the oxidation of 1-phenylethanol using 30% H_2O_2 as a typical benchmark reaction, as shown in Figure 5.

The hollow γ-Fe_2O_3 was found to be the most effective among the catalysts examined, giving turnover number (TON) of 36 and >99% acetophenone selectivity. As expected, Fe_3O_4-coated PS spheres gave poor activity, which was mainly ascribed to its lower exposed surface area. Unfortunately, hollow Fe_3O_4 was also less effective despite its high surface area. In a separate experiment, the reaction of H_2O_2 (30 mM) and the above materials was performed. The H_2O_2 can be almost entirely recovered in the presence of hollow γ-Fe_2O_3, while Fe_3O_4 samples, especially hollow Fe_3O_4, led to the decomposition of H_2O_2 $\{H_2O_2 \rightarrow H_2O + (1/2)O_2\}$. We point out that non-productive decomposition of H_2O_2 over the catalyst itself decreases the catalytic efficiency. Bulk Fe_3O_4 and γ-Fe_2O_3 (particle size $\geq$ 100 nm) showed high selectivity toward acetophenone, but the activities were unsatisfactory. In the presence of nano-γ-Fe_2O_3 which consists of uniform particles of much smaller size (3–5 nm), the attained TON was comparable to that of the hollow γ-Fe_2O_3 but the selectivity was only 35%; benzoic acid and benzyl benzoate were detected as side products, which is well matched with the soluble Fe system. This indicates that the catalytic activity and selectivity gradually approach those obtained with homogeneous Fe systems as the size of Fe_2O_3 decreases, because the extremely small NPs down to molecular size may behave as a homogeneous system. Thus, the higher catalytic activity of the hollow γ-Fe_2O_3 can be explained by the hollow structure, high efficiency in H_2O_2 utilization and suitable particle size responsible for excellent selectivity.

Other advantages of the hollow γ-Fe_2O_3 are easy recovery from the reaction mixture and reusability. Upon completion of the oxidation reaction, the superparamagnetic properties of the hollow γ-Fe_2O_3 can afford a straightforward way of isolating the catalyst. The catalyst was attracted by applying a permanent magnet externally. The recovered catalyst could be recycled in the above oxidation without significant loss of its inherent activity. This characteristic renders the hollow γ-Fe_2O_3 a pivotal contribution to the establishment of environmentally-

acceptable chemical processes, particularly in the industrial and pharmaceutical application of oxidation reactions.

Conclusion

Hollow γ-Fe_2O_3 nanospheres with diameter of 400–500 nm have been synthesized by a simple templating method combined with subsequent thermal treatments and calcinations. Characterization by several physicochemical methods revealed that primary NPs of approximately 10–20 nm in size organized shell structure and the iron oxide phase was γ-Fe_2O_3. The hollow γ-Fe_2O_3 nanospheres can offer a simple and efficient heterogeneous catalyst system for the oxidation of organic compounds using H_2O_2. It exhibited higher catalytic activity than its bulk counterparts and also showed a satisfactory selectivity compared to the nano-γ-Fe_2O_3. Recovery of the catalyst was easily accomplished by external application of a permanent magnet, and the spent catalyst could be recycled. We expect that such multifunctionality including the hollow interiors, unique catalytic function, and magnetic properties will render them ideal candidates for catalytic application.

This work is supported by the Grant-in-Aid for Scientific Research from Ministry of Education, Culture, Sports, Science and Technology of Japan (No. 21760629). We thank Dr. Eiji Taguchi and Prof. Hirotaro Mori at the Research Center for Ultra-High Voltage Electron Microscopy, Osaka University for assistance with TEM measurements. The X-ray adsorption experiments were performed at SPring-8 (prop. No. 2009B1127).

References

1 a) J. P. Wilcoxon, B. L. Abrams, *Chem. Soc. Rev.* **2006**, *35*, 1162. b) J. D. Mackenzie, E. P. Bescher, *Acc. Chem. Res.* **2007**, *40*, 810. c) S. G. Kwon, T. Hyeon, *Acc. Chem. Res.* **2008**, *41*, 1696.

2 a) D. L. Leslie-Pelecky, R. D. Rieke, *Chem. Mater.* **1996**, *8*, 1770. b) M. A. El-Sayed, *Acc. Chem. Res.* **2001**, *34*, 257. c) D. Astruc, F. Lu, J. R. Aranzaes, *Angew. Chem., Int. Ed.* **2005**, *44*, 7852. d) K. Mori, T. Hara, T. Mizugaki, K. Ebitani, K. Kaneda, *J. Am. Chem. Soc.* **2004**, *126*, 10657.

3 M. Králik, A. Biffis, *J. Mol. Catal. A: Chem.* **2001**, *177*, 113.

4 a) R. M. Crooks, M. Zhao, L. Sun, V. Chechik, L. K. Yeung, *Acc. Chem. Res.* **2001**, *34*, 181. b) T. Mizugaki, M. Murata, S. Fukubayashi, T. Mitsudome, K. Jitsukawa, K. Kaneda, *Chem. Commun.* **2008**, 241.

5 R. S. Underhill, G. Liu, *Chem. Mater.* **2000**, *12*, 3633.

6 J. H. Ding, D. L. Gin, *Chem. Mater.* **2000**, *12*, 22.

7 a) F. Caruso, R. A. Caruso, H. Möhwald, *Science* **1998**, *282*, 1111. b) F. Caruso, *Adv. Mater.* **2001**, *13*, 11. c) X. W. Lou, L. A. Archer, Z. Yang, *Adv. Mater.* **2008**, *20*, 3987.

8 a) S.-W. Kim, M. Kim, W. Y. Lee, T. Hyeon, *J. Am. Chem. Soc.* **2002**, *124*, 7642. b) H. Li, Z. Bian, J. Zhu, D. Zhang, G. Li, Y. Huo, H. Li, Y. Lu, *J. Am. Chem. Soc.* **2007**, *129*, 8406. c) S.-W. Cao, Y.-J. Zhu, *J. Phys. Chem. C* **2008**, *112*, 6253. d) H. Li, J. Liu, S. Xie, M. Qiao, W. Dai, Y. Lu, H. Li, *Adv. Funct. Mater.* **2008**, *18*, 3235. e) H. Li, Y. Xu, J. Liu, Q. Zhao, H. Li, *J. Colloid Interface Sci.* **2009**, *334*, 176.

9 a) D. T. Mitchell, S. B. Lee, L. Trofin, N. Li, T. K. Nevanen, H. Söderlund, C. R. Martin, *J. Am. Chem. Soc.* **2002**, *124*, 11864. b) A. D. Dinsmore, M. F. Hsu, M. G. Nikolaides, M. Marquez, A. R. Bausch, D. A. Weitz, *Science* **2002**, *298*, 1006. c) L. M. Qi, J. Li, J. Ma, *Adv. Mater.* **2002**, *14*, 300. d) Q. Peng, Y. Dong, Y. Li, *Angew. Chem., Int. Ed.* **2003**, *42*, 3027.

10 J. Park, K. An, Y. Hwang, J.-G. Park, H.-J. Noh, J.-Y. Kim, J.-H. Park, N.-M. Hwang, T. Hyeon, *Nat. Mater.* **2004**, *3*, 891.

11 A. V. Trunova, R. Meckenstock, I. Barsukov, C. Hassel, O. Margeat, M. Spasova, J. Lindner, M. Farle, *J. Appl. Phys.* **2008**, *104*, 093904.

12 B. Lv, Y. Xu, Q. Gao, D. Wu, Y. Sun, *J. Nanosci. Nanotechnol.* **2010**, *10*, 2348.

13 A. F. Thünemann, J. Kegel, J. Polte, F. Emmerling, *Anal. Chem.* **2008**, *80*, 5905.

14 M. Ozaki, E. Matijević, *J. Colloid Interface Sci.* **1985**, *107*, 199.

15 A. B. Bourlinos, A. Simopoulos, D. Petridis, *Chem. Mater.* **2002**, *14*, 899.

16 Y. S. Kang, S. Risbud, J. F. Rabolt, P. Stroeve, *Chem. Mater.* **1996**, *8*, 2209.

17 a) K. Mori, S. Kanai, T. Hara, T. Mizugaki, K. Ebitani, K. Jitsukawa, K. Kaneda, *Chem. Mater.* **2007**, *19*, 1249. b) K. Mori, Y. Kondo, S. Morimoto, H. Yamashita, *J. Phys. Chem. C* **2008**, *112*, 397.

18 J. W. Long, M. S. Logan, C. P. Rhodes, E. E. Carpenter, R. M. Stroud, D. R. Rolison, *J. Am. Chem. Soc.* **2004**, *126*, 16879.

19 S. Sun, H. Zeng, *J. Am. Chem. Soc.* **2002**, *124*, 8204.

20 a) K. Mori, K. Sugihara, Y. Kondo, T. Takeuchi, S. Morimoto, H. Yamashita, *J. Phys. Chem. C* **2008**, *112*, 16478. b) K. Mori, K. Kagohara, H. Yamashita, *J. Phys. Chem. C* **2008**, *112*, 2593. c) K. Mori, N. Yoshioka, Y. Kondo, T. Takeuchi, H. Yamashita, *Green Chem.* **2009**, *11*, 1337. d) K. Mori, Y. Kondo, H. Yamashita, *Phys. Chem. Chem. Phys.* **2009**, *11*, 8949.

21 M. E. Fleet, *Acta Crystallogr., Sect. B* **1981**, *37*, 917.

22 A. V. Korobeinikova, V. I. Fadeeva, L. A. Reznitskii, *J. Struct. Chem.* **1976**, *17*, 737.

23 J. C. Bart, *Adv. Catal.* **1986**, *34*, 203.

24 H. Yamashita, Y. Ohtsuka, S. Yoshida, A. Tomita, *Energy Fuels* **1989**, *3*, 686.

25 a) S.-T. Wong, J.-F. Lee, S. Cheng, C.-Y. Mou, *Appl. Catal., A* **2000**, *198*, 115. b) T. Liu, L. Guo, Y. Tao, T. D. Hu, Y. N. Xie, J. Zhang, *Nanostruct. Mater.* **1999**, *11*, 1329.

26 P. T. Anastas, J. C. Warner, *Green Chemistry: Theory and Practice*, Oxford University Press, **1998**.